Energy transfers in a weakly coupled gas-surface system: The scattering of CO from MgO(001)

Kai Töpfer, Gernot Füchsel, Jean Christophe Tremblay

Energy Transfers in a Weakly Coupled Gas-Surface System: The Scattering of CO from MgO(001)

Kai Töpfer[a], Gernot Füchsel[a], Jean Christophe Tremblay[b,*]

[a] *Institut für Chemie und Biochemie, Freie Universität Berlin, Arnimallee 22, 14195 Berlin, Germany*
[b] *Laboratoire de Physique et Chimie Théoriques, CNRS/Université de Lorraine, UMR 7019, 1 Bd Arago, 57070 Metz, France*

Abstract

This work reports on quasi-classical dynamics simulations of the non-reactive scattering of CO from a prototypical cubic ionic surface. We shed light on the role of the incidence energy, the initial ro-vibrational state of impinging CO, and the effect of surface atom motion on the scattering behaviour of the molecules. Our results rely on a novel high-dimensional potential energy surface, which is fitted using a modified reactive bond order force field to reproduce reference energy data obtained from periodic embedding density functional theory. The scattering process is found to be strongly influenced by the anisotropy of the potential for CO impinging either from the C-end or O-end of the molecule. The distinct scattering features are significant at low incidence energies when surface atom motion is included in the simulations. This suggests that modelling energy transfer to phonons is very important to describe the dynamics of such weakly interacting systems.

Keywords: Diatom-Surface Scattering, Ionic Surfaces, Force Field, Molecular Dynamics

1. Introduction

Reactions at surfaces play a major role in the chemical industry and, thus, make up an important economic factor in modern societies.[1–3] Investigations of elementary processes in heterogeneous catalysis, such as bond making and breaking, have therefore a long tradition in surface science. In order to understand interfacial interactions, reactive and non-reactive scattering experiments are often performed on gas-surface systems. In particular, molecular beam scattering experiments have a long history as one of the most powerful techniques to study reaction dynamics at the gas-solid interface,[4, 5] because they allow to

*Corresponding author. Tel. +49 3 72 74 92 02 (J.C. Tremblay)
Email address: jean-christophe.tremblay@univ-lorraine.fr (Jean Christophe Tremblay)

investigate the dependence of a chemical reaction on the applied reaction conditions in a well-defined manner. The importance of the initial ro-vibrational state of the incident molecule on its reactivity has often been investigated on systems including diatomic molecules.[6–8] State-to-state scattering experiments performed at non-reactive conditions additionally raise the possibility to screen the topology of the potential energy surface (PES) and to indirectly measure energy transfer processes.[9] The latter are associated with energy redistribution inside the scattered particle and energy transferred to the substrate, and they can be mediated by two different dissipative channels: phononic and electronic. For ionic surfaces, energy loss to phonons is the only available channel at low incident energies.

For one, the catalytic oxidation of CO is an extensively studied reaction because of its importance for converting toxic CO into comparably harmless CO_2. It can be performed under various conditions and using a number of different catalysts. A possibly surprising – and rather exotic choice – is that of gold nanoparticles supported by MgO surfaces, which have been reported to efficiently catalyze this reaction, even in extreme conditions at temperatures down to -70°C.[10] Surfaces serve not only as support material for the reaction but can also modify the electronic properties at the reactive center by inducing partial charge transfer.[11] In the absence of metallic nanoparticles, the MgO support appears chemically inert for oxygen adsorption, and CO is found to have only weak interactions with (001) and (111) facets of MgO.[12] From temperature programmed desorption experiments, the absolute CO-MgO(100) binding energy was reported to range from $E_{\mathrm{ads}} = 0.14\,\mathrm{eV}$[13] to $0.4\,\mathrm{eV}$[14]. These values correlate well with theoretical estimates obtained at the Hartree-Fock level of theory ($E_{\mathrm{ads}} = 0.4\,\mathrm{eV}$[15]) and with density functional theory (from 0 to $0.282\,\mathrm{eV}$, see ref. 16 and references therein).

From previous molecular beam experiments performed on non-reactive scattering of CO from a bare MgO(001) surface,[17] quasi-elastic scattering is found to dominate. This is expected due the weak CO-MgO interaction. The angular scattering distribution takes a cosinus-like dependence[18] and its shape is not much affected by an increase of the surface temperature up to $T_s = 400°\mathrm{C}$. This suggests a short residence time of CO on the surface upon collision, correlating with the weak adsorbate-surface interaction. This is also in accordance with heat of adsorption measurements, which confirms the weak CO-MgO(001) attraction with contributions potentially arising from dipole-polar surface interactions.[19]

In this work, we present the first detailed theoretical investigation of the non-reactive scattering of CO from an ideal MgO(001) surface from a dynamical perspective. We investigate the scattering behaviour at normal incidence for different incident energies and assess the impact of rigid versus movable surface ions on energy transfer processes and internal energy redistribution. A first task in this endeavour is the representation of the interaction potential between the adsorbate and the substrate. This is challenging due to the weak interaction energy and to the face centered cubic structure of the surface with alternating Mg^{2+} and O^{2-} ions, which leads to important corrugation along the surface. Here, we construct a high-dimensional PES adopting a reactive bond order force

field ansatz, which is fitted to *ab initio* reference energy points obtained from periodic electrostatic embedding density functional theory. Quasi-classical initial conditions for the state-to-state scattering dynamics are chosen by sampling specifically, low-lying ro-vibrational states of the CO molecule in the gas phase. Scattering simulations are the performed under various conditions to help understand the energy transfer process from the CO molecules to the MgO(001) substrate, as a prototypical cubic ionic surface. This is achieved by a detailed analysis of the angular scattering distributions and time-of-flight spectra, which reveals the importance of surface atom motion and of the orientation during impact on scattering properties.

The work is organized as follows: In the next section, the methods and models used in this work are presented. In the Results section, important features of the PES are succinctly described, followed by a comparison of the properties of scattered molecules under different simulation conditions. Finally, the results are summarized in the Conclusion section, with a brief outlook to future research.

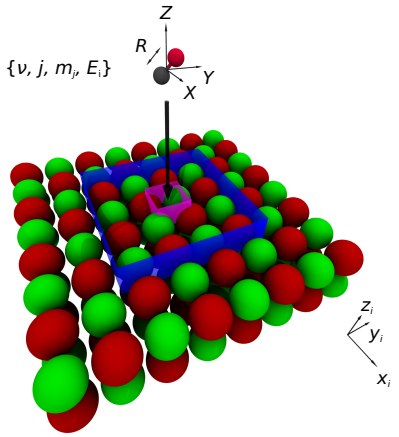

Figure 1: Schematic representation of a CO molecule (red and black beads) approaching a MgO(001) surface (green and red beads). The CO configuration is described by the cartesian position of its center of mass ($\{X, Y, Z\}$), the internal bond length (R), the polar angle Θ relative to the surface normal (not shown), and the azimuthal angle Φ. The surface is described by a first layer of 16 movable ions with cartesian positions $\{x_i, y_i, z_i\}$ (area within the blue box), embedded in a MgO(001) cluster with periodic boundary conditions. The initial conditions for CO are defined by the incident kinetic energy E_i, as well as a quasi-classical ensemble corresponding to the ro-vibrational quantum numbers $\{\nu, j, m_j\}$. The molecule is scattered at normal incidence in the surface area defined by the purple box.

2. Methods and Models

2.1. Potential energy surface construction

The interaction of the molecule with the surface is described in full-dimension, including surface atom displacements. Fig. 1 shows the coordinates used to describe the system dynamics: the cartesian positions of the surface ions subject to periodic boundary conditions in the surface plane, the cartesian coordinates of the CO center of mass (COM), the internal CO bond length R, and the polar and azimuth angles Θ and Φ of the CO adsorbate relative to the surface. Here, we use a modified version of the Reactive Bond Order Force Field (REBO-FF) for gas-surface interaction proposed by Busnengo and co-workers[20], which is based on the potential by Brenner *et al.*[21] The REBO-FF expresses the electronic structure as the sum of repulsive and attractive pairwise atomic interactions, with the chemical environment around the bond treated as three-body terms, the so-called bond-order term. All pairwise interactions are weighted by a smooth cutoff function depending on the distance between the atom pair. An additive non-binding contribution further improves the description of the long range Coulomb force. The simple form of the REBO-FF renders evaluation of the PES efficient, which is important for MD simulations.

In the present work, the bond order term is re-written as a weighted sum of Legendre polynomials for the angular dependency. The motivation for the change is the overall improvement of the root mean square error (RMSE). For a given system, the two-body parameters and the bond order term of the REBO-FF are fitted to reproduce a set of *ab initio* calculations at different geometries (see next section). This is done here by fitting a first set of parameters for the two-body interaction of the individual atoms of the molecule with the surface ions. These parameters serve as initial values for fitting sequentially the three-body and two-body terms for the full molecular interaction with the surface. For the interaction of the atoms of the molecule with those of the surface ions, the pairwise potential is damped in the range from 6.0 Å to 8.4 Å. This accounts for the long-range Coulomb interactions. We note in passing that using a distance-dependent term with $1/r^6$ dispersive asymptotic behaviour did not improve the quality of the REBO-FF fit. The parameters for the intramolecular interaction of CO are further constrained to reproduce the experimental anharmonic vibrational spectrum[22] with a weighting of 2:1 favoring the reproduction of *ab initio* points. The interaction among surface ions is simplified to include only the two-body terms. The Coulomb interaction between surface ions with the same charge is simplified to its repulsive part only. The interaction among the surface ions are smoothly damped in the region from 3.0 Å to 4.7 Å. The detail of these modifications can be found in the Supplementary Information.

As a result of the fitting procedure described above, the PES reproduces *ab initio* data up to an energy of 1.2 eV above the minimum within chemical accuracy (RMSE below 1 kcal/mol on reference points). The PES reproduces all topological features of the reference data, such as the two local adsorption minima atop a Mg^{2+} ion for CO pointing upwards ($E_{\mathrm{ads}} = 0.17\,\mathrm{eV}$) or downwards ($E_{\mathrm{ads}} = 0.08\,\mathrm{eV}$). We define upward CO as a molecule approaching with

the C-end towards the surface, and downward CO as a molecule approaching with the O-end towards the surface. The experimental adsorption energy for CO on a bulk MgO(001) surface ($E_{\mathrm{ads}}^{(\mathrm{exp})} = 0.14\,\mathrm{eV}$[13]) is also found to be close to the value computed with the fitted REBO-FF.

2.2. Reference ab initio data set and sampling

The reference data set used to fit the parameters of the REBO-FF is calculated at the density functional theory level using the B3LYP hybrid functional.[23, 24] We refrain from using any dispersion correction because they overestimate the binding energy of adsorbates in similar systems.[25] The interaction with the surface is computed using the periodic electrostatic embedded cluster method (PEECM).[26] The different structures represented in the data set are generated using the Atomic Simulation Environment.[27] Gas phase carbon monoxide is described by a 6-311+G* basis set of triple zeta quality, sampled by 120 reference points at different bond lengths between $R \in [0.8, 9]$ Å. The MgO(001) surface is simulated by a $Mg_{25}O_{21}$ cluster centered around a Mg^{2+} ion, embedded into a periodic array of point charges. Mg^{2+} and O^{2-} ions of the substrate are described using 6-311G and 6-31+G basis sets, respectively. Using a lattice constant of $L = 4.212\,\text{Å}$ results in a vertical ionic potential of the cluster ($IP_{\mathrm{cluster}} = 6.65\,\mathrm{eV}$) close to the experimental value of $IP_{\mathrm{exp}} = 7.110\,\mathrm{eV}$.[28]

The potential for the surface ions is sampled by displacing two adjacent Mg^{2+} and O^{2-} ions within the cluster in all three cartesian directions by up to 0.4 Å around the equilibrium geometry, amounting to 210 different configurations. The combined system of CO and MgO(001) is sampled at the high-symmetry points in the surface plane $\{X, Y\}$ (Mg^{2+}, O^{2-}, bridge, hollow). The molecule-surface height is sampled in the range $Z \in [2.0, 15]$ Å, and the CO bond length by $R \in [1.0, 1.4]$ Å. The orientation is varied from $\Theta \in [0, 180°]$ in steps of 30° with an azimuthal angle Φ at either 0 or 45°. All configurations with electronic energy larger than 5 eV above the global PES minimum were systematically discarded, amounting to a total of 1500 reference points. A similar sampling strategy along the $\{X, Y, Z\}$ coordinates is used for the interaction of individual C and O atoms on a MgO(001) cluster, leading to about 150 reference points in each case. All electronic structure calculations are performed using the TURBOMOLE 7.1 program package.[29–31]

2.3. Dissipative molecular dynamics

The scattering of CO from MgO(001) is simulated by MD simulation using a full-dimensional analytic PES of the REBO-FF form, including motion of selected surface atoms. Periodic boundary conditions are applied along the directions parallel to the surface. In the dynamics, the surface is represented by a 4x4x1 slab of length 16.848 Å, which is twice as long as the cutoff limit in the REBO-FF potential (8.4 Å). This prevents any double counting of molecule-surface interactions due to periodic boundary conditions. To reduced computational cost, only the top layer ions within the area of the central 2x2 unit cell (16 ions in total) are allowed to move as indicated in Fig. 1. To model irreversible

energy loss to the MgO bulk phonons at 0 K, the momentum p of the movable surface ions is damped at each time step,

$$p' = p \cdot \exp\left(-\tau_\alpha \cdot \Delta t\right) \tag{1}$$

This procedure is similar to a damping of the surface phonons through a generalized Langevin oscillator at 0K[32–34]. The damping rates used in the present work for Mg^{2+} ($\tau_{Mg} = 2.237$ ps) and O^{2-} ($\tau_O = 2.670$ ps) are obtained by fitting the dynamics of a displaced ion in a freely moving slab to a damped harmonic oscillator (see Supplementary Information for details). The equations of motion are integrated numerically using the velocity-Verlet algorithm with a time step of $\Delta t = 0.05$ fs. The maximal total energy deviation for simulation with a rigid surface remains below 1 meV during the whole propagation.

The system is prepared in a series of initial conditions representing different initial translational energies (or incident energy, E_i) for CO are sampled (E_i = [0.05 eV, 0.10 eV, 0.30 eV, 0.50 eV]). For each incident energy, at least 10'000 trajectories are used to sample the quasi-classical initial conditions for a chosen ro-vibrational state of CO. In all simulations, the impinging CO has an initial internal energy, E_{ν,j,m_j}, associated with the ro-vibrational quantum state defined by the vibrational quantum number ν, the total angular momentum quantum number j and the total angular momentum projection quantum number m_j. The distribution is sampled as described in detail elsewhere.[35] The initial orientation of CO in the ro-vibrational ground state ($\nu = 0, j = 0$) is sampled by a spherical distribution, uniform with respect to the polar (Θ) and azimuthal (Φ) angles. The probe molecule always starts at a height of 9.0 Å and with momentum at normal incidence directed towards the surface. The surface temperature is set to $T_s = 0$ K, without zero-point energy (ZPE), by optimizing the ion positions to the minimum of the REBO-FF. All sampled trajectories are distributed above the movable surface ions within the small purple area shown in Fig. 1. Quantum numbers for the final rotational and vibrational states are assigned to the trajectories in the asymptotic region according to a classical binning procedure as used previously in ref. 35. At the incident energies investigated in this work, the weak interaction of CO with MgO(001) is found to be insufficient to excite CO from its initial vibrational ground state.

3. Results and Discussion

3.1. Potential Energy Surface Topology

Figs. 2 and 3 show selected 2D cuts of the PES. The interaction energy between the CO molecule and a MgO(001) surface is mostly determined by the electrostatic interaction between the electron density of CO and the ionic charges of the surface atoms. The typical molecule-surface distance in the interaction region is found between a chemisorption and physisorption, as in the reference *ab initio* data.

Figure 2 reveals a larger corrugation of the potential along angle Θ with CO placed atop the O^{2-} surface ion (bottom left panel) and the bridge site

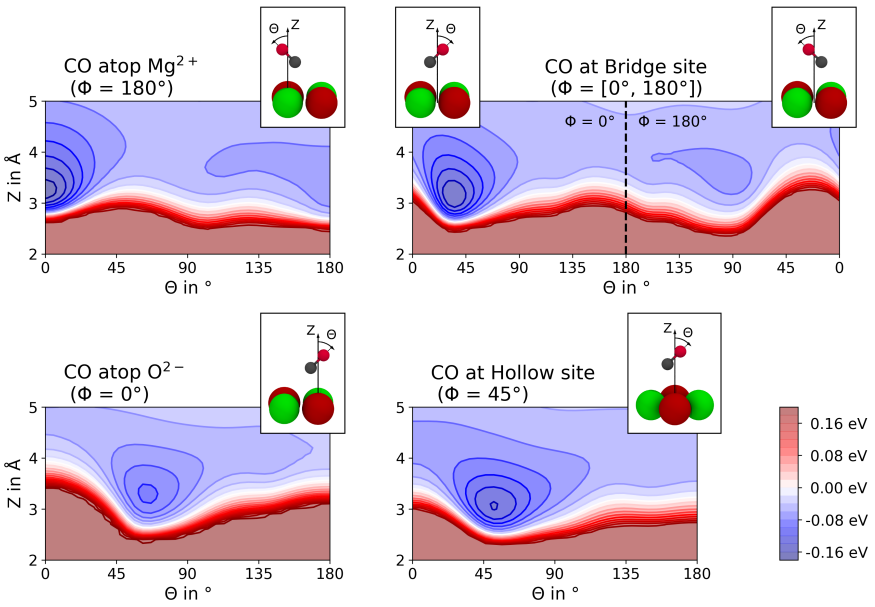

Figure 2: Potential energy surface cuts in the $Z\Theta$-plane. The center of mass of CO is placed atop Mg^{2+} (top left panel), O^{2-} (bottom left panel), at the bridge site (top right panel), and at the hollow site (bottom right panel). A cut-out of the periodic surface with CO ($Z = 3.0$ Å, $\Theta = 45°$) at the respective adsorption site is shown in the right top corner of each panel. The polar angle Θ and associated azimuthal angle Φ is also shown. The CO bond length R is optimized at each point.

(top right panel) than the potential with CO atop Mg^{2+} (top left panel). The minimum positions of the PES atop O^{2-} and the hollow site are around a polar angle Θ of 60° and 50°, respectively, representing a CO molecule pointing with its C atom toward an adjacent Mg^{2+} ion. For CO in the upright position, i.e., with C closer to the surface, the molecule is found in its global potential energy minimum atop the Mg^{2+} ions, while it remains far from the surface above O^{2-} ions. In the downward conformation, a shallow potential minimum is found atop the Mg^{2+} and at the bridge site. The stronger interaction between C and Mg^{2+} ions leads to a preference for a Mg^{2+}–C–O alignment, which explains that the PES minimum at the bridge site is found at about 35° with the oxygen pointing away ($\Phi = 0°$).

Fig. 3 shows the potential surface of CO at different heights in Z along the 1D path in the XY-plane. The path is chosen to sample all important high-symmetry points along the surface, going from Mg^{2+} over the bridge site to O^{2-} and via the hollow site back to Mg^{2+}. The potential cut shows a strong corrugation when CO stands upright (top panel). At $\Theta = 45°$, the PES minimum shifts towards the bridge position, favoring the linear arrangement between Mg^{2+}–C–O. It is interesting to note that the well depth remains almost unchanged. This is indicative of a relatively flat topology around Mg^{2+} ions, as long as the pre-

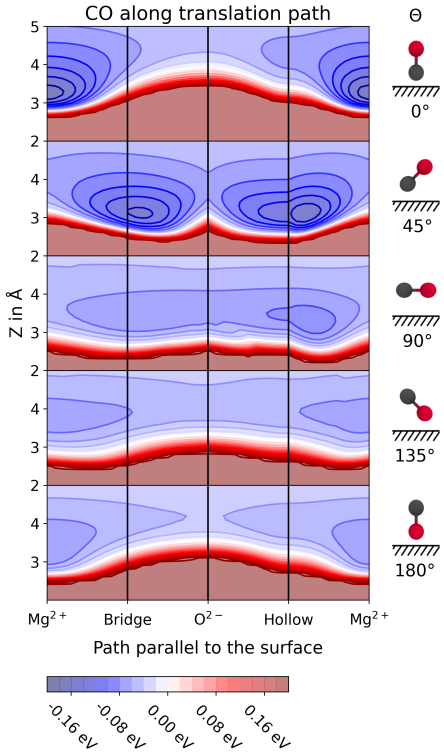

Figure 3: Potential energy surface along Z and a 1D path in the XY-plane of the surface for different angles Θ. The CO bond length R and the angle Φ are optimized at each reference point.

ferred orientation can be adopted. For CO at $\Theta > 90°$, the attractive interaction with the surface becomes weak. The PES is almost flat in the XY-plane when the CO lies parallel to the surface, with some small degree of corrugation when the molecule points downwards. These topological features of the PES reveal a strong orientational dependence and an important corrugation at the surface. Both will be shown below to affect the properties of the scattered molecules in the asymptotic channel.

3.2. Scattering from a Rigid Surface

Fig. 4 shows the translational energy loss (top panels), the rotational excitation probability (central panels), and the scattering angle distribution (bottom panels) for scattering of CO initially in the ro-vibrational ground state ($\nu = 0, j = 0$) from a rigid surface at normal incidence. Simulations for CO($\nu = 0, j = 1$) show similar trends and will not be discussed further (see Supplementary Information for detail). The translational energy loss increases smoothly with higher rotational excitation and a larger energy transfer from the translational degrees of freedom towards rotational ones. No vibrational

excitation is possible due to the very weak molecule-surface interaction and the low initial translational energy, which is much lower than the energy of the CO internal stretch mode vibration ($\sim 2140\,\mathrm{hc/cm}$). As a consequence, all translational energy is converted to rotational motion in the case of a rigid surface. This is confirmed by looking at the average translational energy loss ($\langle \Delta E_\mathrm{i} \rangle$), which is equal to the rotational energy gain ($\langle \Delta E_j \rangle$) at all incoming energies, within the accuracy of the present computational setup.

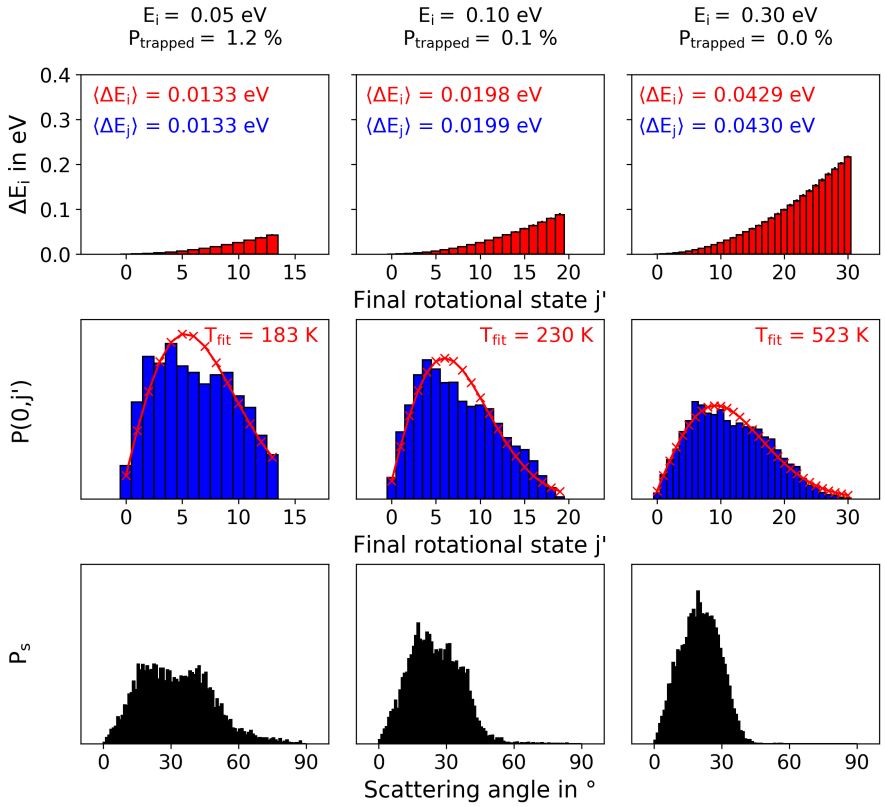

Figure 4: Scattering of CO($\nu = 0, j = 0$) from a rigid MgO(001) surface at different initial translation energies E_i. The trapping probability of CO, P_trapped, is given in the header of each column. Top panels: State-resolved translational energy loss. The average translational energy loss ($\langle \Delta E_\mathrm{i} \rangle$) and average rotational energy gain ($\langle \Delta E_j \rangle$) are given in red and blue, respectively. Central panels: Rotational excitation probability, $P(0, j')$, and best fit to a Boltzmann distribution (red line). Bottom panels: Scattering angle probability distribution.

Although the translation energy loss increases as a function of the initial translational energy, its relative importance decreases. This is due to the weak interaction with the surface and the reduced contact time at higher velocities. The final rotational state and scattering angle distributions in the central and bottom panel in Fig. 4, respectively, reveal a weakly distinct double peak structure at the lowest incident energy. This phenomenon is known as rainbow

scattering and it is here only observed at the lowest incidence energy. The small features in the final rotational state distribution disappears at higher incident energies, as the distributions yield a better agreement with a Boltzmann fit. Two peaks around $\sim 20°$ and $\sim 40°$ can be distinguished from the broad scattering angle distribution at $E_\mathrm{i} = 0.05\,\mathrm{eV}$. While the distribution becomes narrower and the peaks disappears in the intermediate case at $E_\mathrm{i} = 0.10\,\mathrm{eV}$, it gets unimodal, smooth, and narrow at $E_\mathrm{i} = 0.30\,\mathrm{eV}$. Because of the weak molecule-substrate interaction, the effect of the potential topology on the scattering products vanishes rapidly with increasing incident energy. Steering of the molecule to a more favorable orientation upon impact originates from translation-rotation coupling. It is more effective at low collision energies and it can affect reaction probabilities. The trapping probability, P_trapped, observed on the rigid surface at $E_\mathrm{i} = 0.05\,\mathrm{eV}$ due to this type of steering is already very low (1.2 %), and it completely vanishes at higher incidence energies.

To understand the final rotational probability and scattering angle distributions, the role of the impact site and of molecular orientation during impact is investigated. To this end, the surface is divided in areas belonging to Mg^{2+}, to O^{2-}, and to hollow sites, using the effective ionic radii given by Shannon.[36] The effective ionic radii of Mg^{2+} ($r_\mathrm{ionic}(Mg^{2+}) = 0.86\,\text{Å}$) and O^{2-} ($r_\mathrm{ionic}(O^{2-}) = 1.22$ Å) are scaled by a factor of 0.993, such that the sum of both diameters corresponds to the lattice parameter of the unit cell, $L = 4.212$ Å. We count an impact to occur at the first moment when a trajectory yields a sign change in the translational momentum p_z along the z-direction. In the following discussion, this is also referred to the first turning point.

Fig. 5 shows rotational excitation probabilities and scattering angle distributions for trajectories at different impact sites, together with the angular orientation Θ of CO upon impact. At low incident energy ($E_\mathrm{i} = 0.05\,\mathrm{eV}$, left panels) the two peaks observed in the rotational distribution originate from different orientations of CO at the moment of impact. For molecules impinging and scattering from Mg^{2+} ions (top left panels), the peak at lower scattering angles is caused by trajectories where CO is in upward direction, while CO pointing downwards is mostly responsible for the peak at higher angles. At low incident energies, the CO molecule has more time to reorient adiabatically towards an energetically favorable orientation. Guiding the molecule towards the optimal Mg^{2+}–C–O alignment effectively minimizes the force along the angle Θ, as can be seen from the potential curves in Fig. 2. This results in lower rotational excitation and smaller scattering angles for trajectories colliding with Mg^{2+} ions than with O^{2-} ions (central left panels) or on hollow sites (bottom left panels). CO pointing downwards shows a peak at larger scattering angle despite the flat potential topology (bottom panels of Fig. 3). The different scattering angle distributions between the two CO alignments upon impact decreases at larger incident energies (top right panels). While the scattering angles of upright CO slightly increases, downward CO becomes narrower and shifts to lower scattering angles. At the Mg^{2+} impact site, the proportion of upright to downwards collisions remains approximately constant (35% and 65%) at all incident energies.

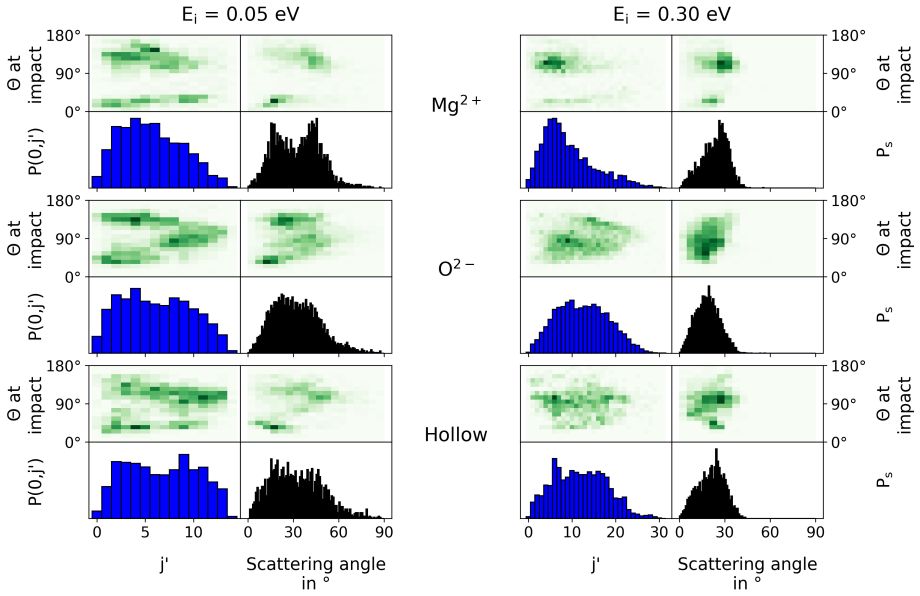

Figure 5: Influence of the impact site and of molecular orientation (Θ of incident CO at the moment of impact) on the j-resolved rotational excitation probability ($P(0, j')$) and the scattering angle distribution P_s. CO($\nu = 0, j = 0$) is scattered from a rigid surface at different initial translational energies $E_\mathrm{i} = \{0.05, 0.30\}$ eV. Results for areas belonging to Mg^{2+}, O^{2-}, and hollow sites are depicted correspondingly from top to bottom.

The trajectories at the O^{2-} impact site (central panels of Fig. 5) show a more uniform, non-thermal distribution of the rotational excitation probability ($P(0, j')$). Similar to dynamics at the Mg^{2+} impact site at low incident energies, CO molecules impinging in upright orientation yield lower scattering angles, whereas downward CO molecules scatter at larger angles. Molecules oriented parallel to the surface also tend to scatter at larger angles and to become rotationally more excited. This is a consequence of the PES topology: The coupling between rotational and lateral motion causes larger scattering angles despite the flat potential around O^{2-} (central panel of Fig. 3). At higher incident energies, this effect vanishes and both the rotational excitation probability and the scattering angle distribution become narrower due to the reduced contact time with the surface.

Trajectories of CO molecules impinging at the hollow site show a similar but broader rotational excitation probability as those at the O^{2-} impact sites. On the other hand, the scattering angle distribution is found between that of the two ionic sites. The azimuthal angle Φ has a large impact on the surface topology for non-perpendicular CO molecules at the hollow site. The potential character changes from strongly attractive if CO aligns towards two Mg^{2+} (i.e. $\Phi = 45°$ as shown in the bottom right panel of Fig. 2) to weakly bound when aligning towards an O^{2-} ions (i.e. $\Phi = 135°$). At higher incident energy (bottom

right panels in Fig.5), the scattering angle distribution becomes narrower and the rotational excitation probability becomes almost indistinguishable from that at the O^{2-} site. All subtle effects stemming from the PES corrugation are lost, while they are still visible at the Mg^{2+} site.

3.3. Influence of Surface Ion Motion

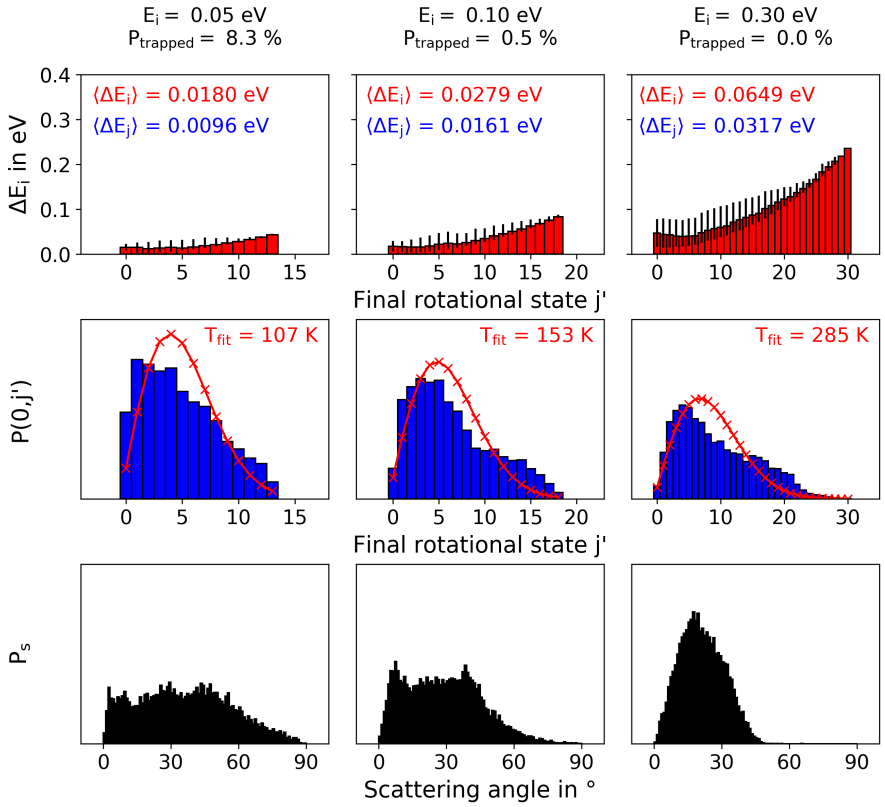

Figure 6: Scattering of CO($\nu = 0, j = 0$) from a MgO(001) surface including surface atom motion at different initial translation energies E_i. The trapping probability of CO, P_trapped, is given in the header of each column. Top panels: State-resolved translational energy loss. The average translational energy loss ($\langle \Delta E_i \rangle$) with standard deviation and average rotational energy gain ($\langle \Delta E_j \rangle$) are given in red and blue, respectively. The standard deviation for the binning is shown as black bars. Central panels: Rotational excitation probability, $P(0, j')$, and best fit to a Boltzmann distribution (red line). Bottom panels: Scattering angle probability distribution.

Fig. 6 shows the rotational excitation probability and scattering angle distribution for different incident energies E_i including surface ion motion. Unsurprisingly, the loss of initial translational energy is larger for scattering on a movable surface. On the other hand, the average rotational energy gain gets smaller than on a rigid surface and amounts to about half of the translational

energy loss for all incoming energies studied. The remaining translational energy goes into the surface ion motion. Consequently, excitation probability of lower rotational states becomes more likely and the distribution is shifted to the left (see central panels). This observation remains valid at larger incident energies. The excitation probability distributions deviate more strongly from the ideal Boltzmann case (red curve), but the associated temperatures are much lower than for scattering from a rigid surfaces. As a novel feature, a shoulder in the rotational distributions can be observed at higher js for all initial translational energies. Such a shoulder is not observed in the scattering angle distributions, which is also broader at low incident energies when surface ions are allowed to move. The distribution for $E_\mathrm{i} = 0.30\,\mathrm{eV}$ is close to the scattering angle distribution on a rigid surface. This is possibly due to the diminishing contact time and the long lifetime of surface phonons, as can be inferred from the ion damping rate in Eq.(1). The trapping probability P_trapped is only significant at low impinging energies (8.3 % at $E_\mathrm{i} = 0.05\,\mathrm{eV}$). The steering effect on a surface with movable ions appears to significantly increase the trapping probability at such low incident energies. While it is also increased at $E_\mathrm{i} = 0.10\,\mathrm{eV}$ compared with rigid surface simulations (0.5 % versus 0.1 %), energy loss to phonons does not significantly enhance trapping. This result can again be understood from the damping rates in the cluster. They operate on the few picosecond regime, which is much longer than the contact time during the scattering event. Note that the trapping probabilities should be taken with caution, since they are computed classically and neglect the zero-point energy of the system.

To shed light on the origin of the structure of the distributions, the left panels of Fig. 7 show rotational excitation probability and scattering angle distribution for different impact sites at the surface. The probabilities are further decomposed according to the CO orientation Θ upon impact. As opposed to Fig. 5 the scattering angle distribution (black) at the Mg^{2+} impact site exhibits an intense and narrow peak at small angles. According to the impact angle (green colormap), it is associated with CO approaching the surface in an upright orientation. This is associated with a rotational distribution (blue) that is markedly skewed towards low js, with an important dip at $j' = 0$. This strong localization can be explained as follows: as CO approaches the surface at low incident velocities, it is dragged towards the Mg^{2+} surface ion, which is pushed below the first surface layer upon impact. This constrains the motion of the CO projectile by creating a stronger confinement potential than on a rigid surface. This cone-shaped potential and large loss in translational energy of CO prevents deviation of the scattered products from normal incidence. It further restricts rotational motion and confers a large degree of orientation to the scattered molecules. The lower adsorption minimum for CO pointing downwards lead to a lower degree of localization. Consequently, the associated rotational excitation probability and scattering angle distribution behave more thermally. Simulations at higher incident energies behave similarly and are shown in the supplementary material.

The trajectories scattering around the O^{2-} impact site (central left panels) also exhibit rotational cooling as compared to simulations on the rigid surface.

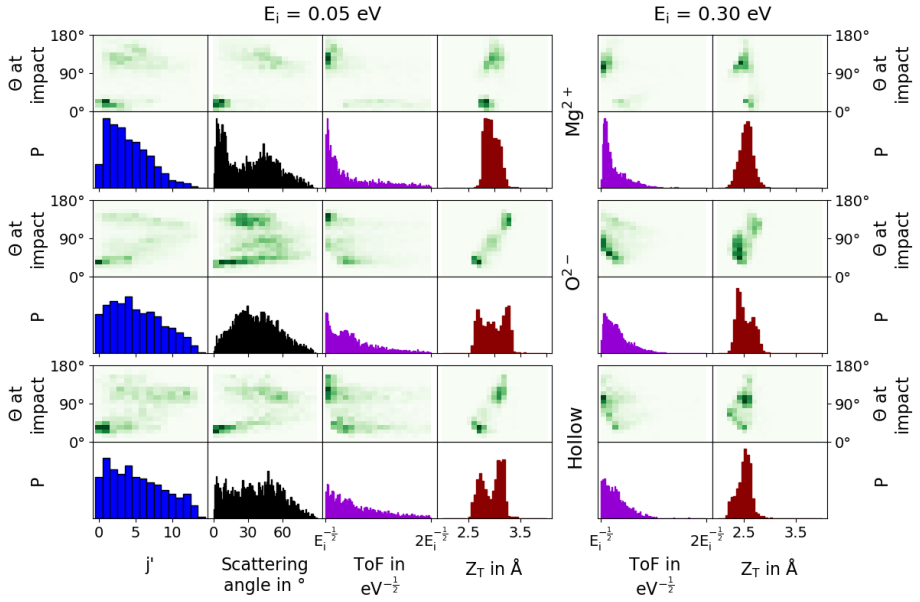

Figure 7: Site-resolved scattering of CO($\nu = 0, j = 0$) from a surface with movable surface ions. Left panels: Rotational excitation probability and scattering angle distribution at different impact sites. (top: Mg^{2+}, centre: O^{2-}, bottom: hollow) for an incident translational energy of $E_i = 0.05\,\text{eV}$. The decomposition according to the CO orientation Θ at the moment of impact is shown in the green density maps. Central and left panels: Time of flight spectra (ToF, purple) and position of the Z turning point upon impact (Z_T) at different incident energies ($E_i = \{0.05, 0.30\}\,\text{eV}$).

Upright CO is more strongly represented at low js. As on the rigid surface, rotational excitation is lower for downward CO upon impact, while a parallel alignment results into larger values in j. Trajectories with low scattering angles correlate well with the energetically optimal Θ angle of CO at the moment of impact, corresponding to the minimum structure at the bridge and O^{2-} site (see Fig. 3). As it is also observed at the Mg^{2+} site, surface ion motion leads to a more efficient reorientation of CO towards the energetic minimum structures. This subsequently increases the probability of excitation to low rotational states and small scattering angles due to a larger energy transfer from the impinging CO molecule towards the surface. The influence of the impact orientation on the rotational transition probability and scattering angle distribution remains otherwise qualitatively similar to the rigid surface simulations. The same observation can be made for the remaining trajectories around the hollow site. The general trends are thus strongly dominated by the topology of the potential, despite the low interaction energy.

Further information about the energy transfer to the surface can be obtained from the time of flight (ToF) spectra, which are inversely proportional to the translation kinetic energy of the scattered molecules. It is shown in the central

and right panels of Fig. 7 (purple), along with the position of the Z turning point upon impact (Z_{T}, brown). The ToF spectra reveal an important loss of translational energy when CO molecules hit the surface pointing upwards. This observation holds for all simulated incident energies and impact areas, and it is a signature of internal energy redistribution. Scatterers adopting another orientation upon impact are less thwarted in their motion and retain more kinetic energy in the exit channel. Consequently, they should be observed first in a ToF spectrum. While all impact sites have a relatively similar profiles, the separation between upright and downwards orientations is larger for collision at the Mg^{2+} site. This confirms that scattering in the downwards orientation is a more direct and more adiabatic process. CO scattering in upright orientation is a more inelastic process and the large kinetic energy loss towards the surface enhance the rotational cooling and lower the scattering angle deviation.

At low incidence energies, the turning point Z_{T} indicates that scattering happens further away from the surface for the downwards orientation, while scattering closer to the surface is observed for CO molecules incoming in an upright orientation. This can be understood from the topological feature of the PES (see Fig. 2). CO reaches a more repulsive potential later at lower distances Z from the surface around hollow and O^{2-} impact sites when it is pointing approximately upwards. Adopting a $\Theta < 90°$ orientation, CO goes through a potential minimum valley with a late repulsive potential. Impinging molecules in a downward orientation ($\Theta > 90°$) have either a shallow or no potential minimum and reach the repulsive wall of the PES at higher Z distances from the surface, which amounts to a second peak in the distributions. This trend is reversed at higher incident energies (right panels of Fig. 7) for trajectories impinging at the Mg^{2+} site, when CO has less time to adopt an optimal orientation. While the distribution of orientations upon impact becomes narrower for the hollow and O^{2-} impact sites, the two peaks can still be distinguished at the Mg^{2+} site due to deeper PES minima. At higher incident energies, CO molecules approach closer to the surface without significantly transferring energy to the long-lived phonons due to the reduced contact time and the weak interaction with the surface. The molecules thus fly above the interaction potential and reach, almost undisturbed in their initial orientation, the repulsive potential wall. The latter is found to be slightly closer to the surface for CO in the downwards orientation. The low turning point and later scattering of CO molecules in the upright orientation is in contradiction with experimental findings in other systems, where a narrow scattering is observed for early scattering trajectories.[37] We presume that this difference is at least in part due to the fact that MgO(001) presents two types of surface ions.

Translational energy transfer from the impinging molecule to the surface depends on the mass of the projectile and the impact site. In the Baule model[38], translational energy loss Δ is cast as a function of the adsorption energy and of the mass ratio $\mu = m_{\mathrm{ads}}/M_{\mathrm{site}}$ between the molecule and associated the surface atom

$$\Delta = \frac{4\mu}{(1+\mu)^2}\left(E_{\mathrm{i}} + E_{\mathrm{ads}} - \frac{1}{2}k_B T_{\mathrm{s}}\right) \tag{2}$$

The prefactor for the collisions at the O^{2-} site is slightly smaller than on Mg^{2+} (0.926 vs. 0.995). At low incident energy, this can be compensated by the small adsorption energy in the different conformations. For CO on MgO(001), stable adsorption minima are observed on Mg^{2+} in both the upright (0.17 eV) and downward (0.08 eV) orientations. CO atop O^{2-} adopts a meta-stable adsorption state (0.09 eV) by keeping the favorably tilted Mg^{2+}–C–O alignment. For CO in the upright orientation impinging on the Mg^{2+} site, Eq. (2) predicts the largest translational energy loss ($\Delta_{\mathrm{Mg-CO}} = 0.21\,\mathrm{eV}$ at $E_\mathrm{i} = 0.05\,\mathrm{eV}$, and $\Delta_{\mathrm{Mg-CO}} = 0.46\,\mathrm{eV}$ at $E_\mathrm{i} = 0.30\,\mathrm{eV}$). The ToF spectrum confirms that the energy loss for CO molecules adopting an upright orientation is much larger than for the downward orientation. The mass ratio being equal, this finding is in agreement with the higher adsorption energy for the upright orientation. At low incident energy, the Baule model further predicts a minimally larger translational energy loss for upright CO at the O^{2-} site ($\Delta_{\mathrm{O-CO}} = 0.13\,\mathrm{eV}$) than for CO molecules impinging downwards at the Mg^{2+} site ($\Delta_{\mathrm{Mg-CO}} = 0.12\,\mathrm{eV}$). This effect is visible in the broader rotational distribution and in the longer ToF at the O^{2-} site (see left and central panels of Fig. 7). As the incident energy E_i increases, these differences rapidly become smaller, since the contribution of the adsorption energy in Eq. (2) diminishes. Consequently, the trends are almost reversed due to the larger prefactor for the collision on Mg^{2+} ($\Delta_{\mathrm{O-CO}} = 0.361\,\mathrm{eV}$ vs. $\Delta_{\mathrm{Mg-CO}} = 0.358\,\mathrm{eV}$ at $E_\mathrm{i} = 0.3\,\mathrm{eV}$). Similar findings were made by Kondo and coworkers from scattering experiments of CO on LiF(001).[39] LiF has the same rock salt surface structure as MgO but lower ionic charges and shows a gas-surface potential with comparably shallow adsorption minima. They conclude, that scattering of downwards CO experience a more elastic scattering, where the scattering induces only a small transfer of translational energy to the surface. Scattering of upwards CO results more often in trapping and multiple collisions on the surface. The latter is in agreement with our simulations, which reveal a large translational energy loss for upwards CO, independently of the impact site.

4. Conclusion

This works reports on simulations of state-resolved CO scattering from an ionic MgO(001) surface at normal incidence, as a case study for weakly interacting gas-surface system. A new global potential energy surface for the CO/MgO(001) system is adjusted to a modified reactive bond order force field form, which is parameterized to new reference energy values from periodic cluster embedding DFT-calculations. The shallow adsorption minimum of perpendicular CO atop a Mg^{2+} ion is close to the experimentally observed result. The optimized force field is accurate, capturing the subtleties of the weak gas-surface interaction up to potential energies of 1.2 eV above the potential minimum. The impact of energy transfer to the surface phonons on the scattering behaviour of impinging CO is investigated by further parametrizing the force field to include surface ion motion. Irreversible dissipation of the surface energy is included by

damping the motion of the surface atoms, which are found to have relatively long lifetimes on the order of the picoseconds.

The scattering behaviour of CO molecules is found to depend strongly on the orientation of CO upon impact, especially for collisions around Mg^{2+}. An energetically more optimal Mg^{2+}–C–O alignment results in lower rotational excitation and smaller scattering angles. Parallel and downwards CO molecules shows larger rotational excitation and higher scattering angles. Energy transfer to the surface ions increases the probability of lower rotational excitation and smaller scattering angles, which correlates with the additional translational energy loss of CO towards the surface. This allows the thwarted CO molecules to adopt an energetically more optimal alignment during impact, leading to an even narrower distribution at lower final rotational states and scattering angles. At incident energies larger than the adsorption depth, energy transfer to the surface becomes less efficient and scattering behaves as though on a rigid surface.

The observed energy transfer is well rationalized using the Baule model, as a subtle interplay between weak adsorption and energy transfer efficiency factors. While the mass ratio between CO and both surface ion types have a minor influence on the energy transfer rate, the potential depth for the different impact orientations mainly determines the energy transfer. The case of CO scattering from MgO(001), a surface with similar mass ratios for different impact sites, shows the importance of the potential energy topology on the scattering behaviour. An energetically optimal impact orientation amounts to late scattering with larger CO energy loss, lower rotational excitation, and smaller scattering angles. Early scattering for other orientations results in a larger energy transfer towards rotational and lateral movements. The findings demonstrate that the CO scattering from MgO(001) at low incidence energies would provide a rich, yet challenging test systems for experimental measurements of weakly interacting gas-surface systems.

5. Acknowledgements

This work was partially supported by the Deutsche Forschungsgemeinschaft through project TR 1109/2-1. The computer facilities of the Freie Universität Berlin (ZEDAT) are acknowledged for computer time.

References

[1] I. Chorkendorff, J. W. Niemantsverdriet, Concepts of Modern Catalysis and Kinetics, 3rd Edition, Wiley-VCH, 2017.

[2] S. Wacławek, V. V. T. Padil, M. Černík, Major Advances and Challenges in Heterogeneous Catalysis for Environmental Applications: A Review, Ecol. Chem. Eng. S 25 (1) (2018) 9–34.

[3] S. Dang, H. Yang, P. Gao, H. Wang, X. Li, W. Wei, Y. Sun, A Review of Research Progress on Heterogeneous Catalysts for Methanol Synthesis from Carbon Dioxide Hydrogenation, Catal. Today 330 (2019) 61–75.

[4] G. Comsa, Surface Scattering of Thermal Energy He Beams: From the Proof of the Wave nature of Atoms to a Versatile and Efficient Surface probe, Surf. Sci. 300 (1994) 77–91.

[5] J. Libuda, H.-J. Freund, Molecular Beam Experiments on Model Catalysts, Surf. Sci. Rep. 57 (7) (2005) 157–298.

[6] A. W. Kleyn, Molecular beams and Chemical Dnamics at Surfaces, Chem. Soc. Rev. 32 (2003) 87–95.

[7] R. B. Gerber, Molecular Scattering From Surfaces: Theoretical Methods and Results, Chem. Rev. 87 (1) (1987) 29–79.

[8] G.-J. Kroes, C. Díaz, Quantum and Classical Dynamics of Reactive Scattering of H_2 From Metal Surfaces, Chem. Soc. Rev. 45 (2016) 3658–3700.

[9] A. M. Wodtke, Electronically Non-Adiabatic Influences in Surface Chemistry and Dynamics, Chem. Soc. Rev. 45 (2016) 3641–3657.

[10] M. Haruta, Size- and Support-Dependency in the Catalysis of Gold, Catal. Today 36 (1) (1997) 153–166, copper, Silver and Gold in Catalysis.

[11] N. M. Julkapli, S. Bagheri, Magnesium Oxide as a Heterogeneous Catalyst Support, Rev. Inorg. Chem. 36 (1) (2015) 1–41.

[12] C. Duriez, C. Chapon, C. R. Henry, J. M. Rickard, Structural Characterization of MgO(100) Surfaces, Surf. Sci. 230 (1) (1990) 123–136.

[13] R. Wichtendahl, M. Rodriguez-Rodrigo, U. Härtel, H. Kuhlenbeck, H.-J. Freund, Thermodesorption of CO and NO From Vacuum-Cleaved NiO(100) and MgO(100), Phys. Status Solidi A 173 (1) (1999) 93–100.

[14] H. Jian-Wei, C. A. Estrada, J. S. Corneille, W. Ming-Cheng, D. W. Goodman, CO Adsorption on Ultrathin MgO Films Grown on a Mo(100) Surface: An IRAS Study, Surf. Sci. 261 (1) (1992) 164–170.

[15] E. A. Colbourn, W. C. Mackrodt, A Theoretical Study of CO Chemisorption at {001} Surfaces of Non-Defective and Doped MgO, Surf. Sci. 143 (2) (1984) 391–410.

[16] C. Quintanar, R. Caballero, V. M. Castaño, Adsorption of CO on the Rumpled MgO(100), MgO(100):Ni, and MgO(100):Cr Surfaces: A Density Functional Approach, Int. J. Quantum Chem. 102 (5) (2005) 820–828.

[17] C. R. Henry, C. Chapon, C. Duriez, Precursor State in the Chemisorption of CO on Supported Palladium Clusters, J. Chem. Phys. 95 (1) (1991) 700–705.

[18] C. R. Henry, C. Chapon, C. Duriez, Physics and Chemistry of Small Clusters, Vol. 158, NATO ASI Series (Plenum Press, New York), 1987, Ch. Molecular Beam Relaxation Spectroscopy Applied to Adsorption Kinetics on Small Supported Catalyst Particles, pp. 795–800.

[19] S. Furuyama, H. Fujii, M. Kawamura, T. Morimoto, Physisorption of Nitric Oxide, Carbon Monoxide, Nitrogen, and Oxygen by Magnesium Oxide Powder, J. Phys. Chem. 82 (9) (1978) 1028–1032.

[20] Y. Xiao, W. Dong, H. F. Busnengo, Reactive Force Fields for Surface Chemical Reactions: A Case Study with Hydrogen Dissociation on Pd Surfaces, J. Chem. Phys. 132 (1) (2010) 014704.

[21] D. W. Brenner, O. A. Shenderova, J. A. Harrison, S. J. Stuart, B. Ni, S. B. Sinnott, A Second-Generation Reactive Empirical Bond Order (REBO) Potential Energy Expression for Hydrocarbons, J. Phys. Condens. Matter 14 (4) (2002) 783–802.

[22] CRC Handbook, CRC Handbook of Chemistry and Physics, 85th Edition, 85th Edition, CRC Press, 2004.

[23] A. D. Becke, Density Functional Thermochemistry. III. The Role of Exact Exchange, J. Chem. Phys. 98 (7) (1993) 5648–5652.

[24] C. Lee, W. Yang, R. G. Parr, Development of the Colle-Salvetti Correlation-Energy Formula into a Functional of the Electron Density, Phys. Rev. B 37 (1988) 785–789.

[25] S. Ehrlich, J. Moellmann, W. Reckien, T. Bredow, S. Grimme, System-Dependent Dispersion Coefficients for the DFT-D3 Treatment of Adsorption Processes on Ionic Surfaces, ChemPhysChem 12 (17) (2011) 3414–3420.

[26] A. M. Burow, M. Sierka, J. Döbler, J. Sauer, Point Defects in CaF_2 and CeO_2 Investigated by the Periodic Electrostatic Embedded Cluster Method, J. Chem. Phys. 130 (17) (2009) 174710.

[27] S. R. Bahn, K. W. Jacobsen, An Object-Oriented Scripting Interface to a Legacy Electronic Structure Code, Comput. Sci. Eng. 4 (3) (2002) 56–66.

[28] S. Heo, E. Cho, H.-I. Lee, G. S. Park, H. J. Kang, T. Nagatomi, P. Choi, B.-D. Choi, Band Gap and Defect States of MgO Thin Films Investigated Using Reflection Electron Energy Loss Spectroscopy, AIP Adv. 5 (7) (2015) 077167.

[29] R. Ahlrichs, M. Bär, M. Häser, H. Horn, C. Kölmel, Electronic Structure Calculations on Workstation Computers: The Program System TURBOMOLE, Chem. Phys. Lett. 162 (3) (1989) 165–169.

[30] O. Treutler, R. Ahlrichs, Efficient Molecular Numerical Integration Schemes, J. Chem. Phys. 102 (1) (1995) 346–354.

[31] M. Von Arnim, R. Ahlrichs, Performance of Parallel TURBOMOLE for Density Functional Calculations, J. Comput. Chem. 19 (15) (1998) 1746–1757.

[32] S. Adelman, J. Doll, Generalized Langevin Equation Approach for Atom/Solid-Surface Scattering: General Formulation for Classical Scattering Off Harmonic Solids, J. Chem. Phys. 64 (6) (1976) 2375–2388.

[33] J. Tully, Dynamics of Gas–Surface Interactions: 3D Generalized Langevin Model Applied to fcc and bcc Surfaces, J. Chem. Phys. 73 (4) (1980) 1975–1985.

[34] H. Busnengo, A. Salin, W. Dong, Representation of the 6D Potential Energy Surface for a Diatomic Molecule Near a Solid Surface, J. Chem. Phys. 112 (17) (2000) 7641–7651.

[35] G. Füchsel, X. Zhou, B. Jiang, J. I. Juaristi, M. Alducin, H. Guo, G.-J. Kroes, Reactive and Nonreactive Scattering of HCl From Au (111): An ab initio Molecular Dynamics study, J. Phys. Chem. C 123 (4) (2019) 2287–2299.

[36] R. D. Shannon, Revised Effective Ionic Radii and Systematic Studies of Interatomic Distances in Halides and Chalcogenides, Acta Crystallogr. A 32 (5) (1976) 751–767.

[37] I. Lončarić, G. Füchsel, J. I. Juaristi, P. Saalfrank, Strong Anisotropic Interaction Controls Unusual Sticking and Scattering of CO at Ru(0001), Phys. Rev. Lett. 119 (2017) 146101.

[38] A. Groß, Theoretical Surface Science - A Microscopic Perspective, 2nd Edition, Springer Science, Berlin Heidelberg, 2009.

[39] T. Kondo, H. S. Kato, T. Yamada, S. Yamamoto, M. Kawai, Rainbow Scattering of CO and N_2 from LiF(001), J. Chem. Phys. 122 (24) (2005) 244713.

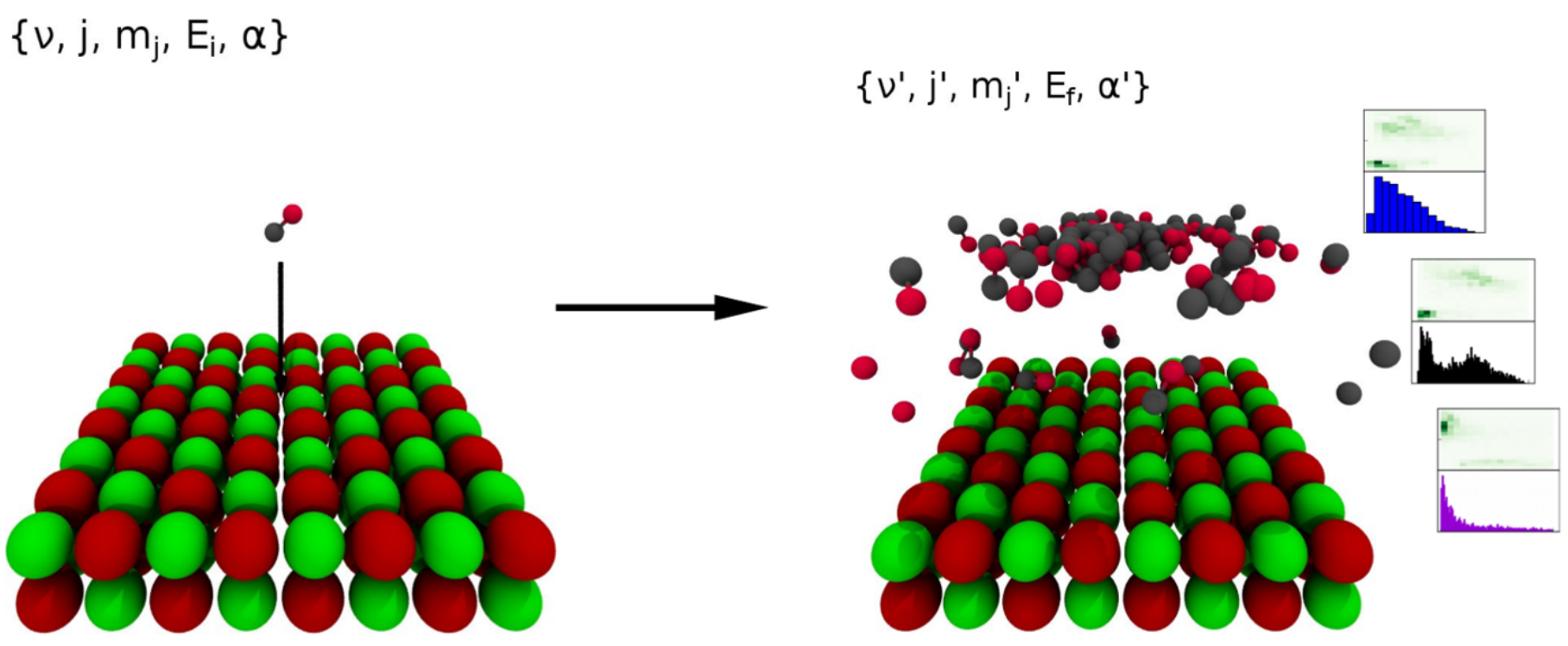
{ν, j, m_j, E_i, α}
{ν', j', m_j', E_f, α'}